Physica B 658 (2023) 414821

Contents lists available at ScienceDirect

Physica B: Condensed Matter

journal homepage: www.elsevier.com/locate/physb

Magnetic ordering and chirality in multiferroic $Dy_{1-x}Ho_xMnO_3$ (x = 0.2)

A.N. Matveeva [a,*,1], I.A. Zobkalo [a], A. Sazonov [b,1], A.L. Freidman [c,d], S.V. Semenov [c,d], M.I. Kolkov [c], K. Yu Terentjev [c], N.S. Pavlovskiy [c], K.A. Shaykhutdinov [c,d], V. Hutanu [b,2]

[a] Petersburg Nuclear Physics Institute by B.P. Konstantinov of NRC «Kurchatov Institute», 188300, Gatchina, Russia
[b] Institute of Crystallography, RWTH Aachen University and Jülich Centre for Neutron Science at Heinz Maier- Leibnitz Zentrum, Garching, Germany
[c] Kirensky Institute of Physics, Federal Research Center, Krasnoyarsk, 660036, Russia
[d] Siberian Federal University, Krasnoyarsk, 660041, Russia

ARTICLE INFO

Keywords:
Neutron diffraction
Crystal structure
Multiferroics
Magnetic structure
Manganites

ABSTRACT

Effect of substitution Dy by Ho on the magneto-electric behavior of the compound $Dy_{0.8}Ho_{0.2}MnO_3$ was investigated by the different methods of polarized and classical neutron diffraction and macroscopic methods. It is shown that substitution by Ho of 20% on the position of Dy do not change overall crystal symmetry of compound. It remains of *Pbnm* type down to the very low temperatures. Magnetic ordering, its temperature and field evolution was determined by the use of single crystal neutron diffraction and magnetization measurements. Chiral type of magnetic structure on Mn subsystem is confirmed below Tc ≈ 16 K. Using polarized neutron diffraction the 3-component character of rare earth magnetic ordering in $Dy_{0.8}Ho_{0.2}MnO_3$ in contrast to $DyMnO_3$ could be revealed. It was shown that doping by 20% Ho suppresses the spontaneous rare-earth ordering with its own propagation vector and provides the situation when two magnetic subsystems, manganese and rare earth ones have a coherent incommensurate spatial propagation. The influence of the external electric field on the magnetic chirality could be directly evidenced, proving strong magneto-electric coupling in multiferroic phase. The study of the electric polarization under similar temperatures and fields on the same samples provides the direct correlation between the results of the microscopic and macroscopic investigations.

1. Introduction

Multiferroics of type II demonstrate strong interaction between magnetic and ferroelectric order parameters, which is manifested in particular in the induction of ferroelectric polarization by a certain type of magnetic ordering. This coupling also leads to a high sensitivity of the dielectric properties to external magnetic fields. Orthorhombic manganites family $RMnO_3$ (R = Tb, Dy, Gd, Ho, Y) are considered to be a typical representatives of the multiferroics of the type II [1–6]. These are isostructrural compounds, which crystalize in the space group # 62, which is more often considered in *Pbnm* setting. Notwithstanding on the similarity in the crystal structure for compounds with R = Tb, Dy from one side and Ho, Y from another side, there are significant differences in their magnetic ordering and supposed mechanisms of multiferroicity.

Long range magnetic order in these compounds established at Néel temperatures in the range of T_N = 38 K ÷ 42 K by the alignment of magnetic moments of Mn^{3+} ions in longitudinal spin density wave structure (LSDW) [7–10]. For $DyMnO_3$ (DMO) compound an additional transition from non-chiral longitudinal spin density wave modulation to the chiral cycloidal-type structure takes place at T_{Ch} = 19 K [3,11], the similar situation was observed for $TbMnO_3$ at T_{Ch} = 28 K [7]. Remarkably the emergence of ferroelectric order in $DyMnO_3$ and $TbMnO_3$ coincides with the transition of the Mn magnetic order from the non-chiral type to the chiral one. The magnetic ordering in $HoMnO_3$ changes from LSDW-type to an antiferromagnetic structure of E-type i.e. an up-up-down-down order at temperature of about 27 K [12]. In $YMnO_3$ magnetic structure undergoes lock-in transition at T = 28.7 K [9] remaining in non-commensurate LSDW-modulated E-type antiferromagnetic structure down to lowest temperatures [10].

The emergence of ferroelectric polarization in $DyMnO_3$ and $TbMnO_3$ induced by the cycloidal magnetic structure rather well described by the inverse Dzyaloshinsky-Moria (DMI) model [13,14], where manganese spin system is considered only. At the same time, the polarization studies reveal significant polarization enhancement when rare earth (RE)

* Corresponding author. Leningradskaya oblast, Gatchina, 1, mkr. Orlova roshcha, PNPI, 188300, Russia.
E-mail address: matveeva_an@pnpi.nrcki.ru (A.N. Matveeva).
[1] Current affiliation: ESS Data Management & Software Centre (DMSC), 2200 Copenhagen, Denmark.
[2] Current affiliation: Technical University of Munich, ZWE FRM II, 85748 Garching, Germany.

https://doi.org/10.1016/j.physb.2023.414821
Received 14 February 2023; Received in revised form 13 March 2023; Accepted 16 March 2023
Available online 22 March 2023

magnetic subsystem becomes polarized by manganese one. This polarization takes place at comparatively high temperatures (close to T_{Ch}) and induced RE magnetic structure has the same propagation vector, as the Mn one: $\boldsymbol{k} = (0\ k_y\ 0)$. The Dy^{3+} spontaneous ordering at $DyMnO_3$ takes place into a commensurate antiferromagnetic structure $\boldsymbol{k_{Dy}} = (0\ 1/2\ 0)$ at low temperatures, and this reduces the ferroelectric polarization significantly [3]. This is indication that additional mechanism of ferroelectric polarization should be involved at $DyMnO_3$ and $TbMnO_3$ compounds [15–18]. That is, the total polarization along the *c*-axis emerges due to two different microscopic mechanisms: from the action of inverse DMI between the Mn ions and from the symmetric exchange-striction between the Dy and Mn sublattices. In this case the coherence of the propagation of Mn^{3+} and R^{3+} magnetic phases plays a significant role in inducing the polarization of the symmetric exchange-striction origin [16–18]. The chiral incommensurate magnetic ordering of manganese sublattice in $DyMnO_3$ induces a ferroelectric polarization, the exchange-striction mechanism provides the enhancement of the resulting polarization similar to the situation proposed for the RMn_2O_5 manganates [19]. After formation of the commensurate magnetic (CM) order of the Dy sublattice below T_N^{Dy}, electric polarization is strongly suppressed, thus confirming the importance of the Mn–Dy interactions as the driving mechanism in the polarization enhancement.

In $HoMnO_3$ the strong Ho^{3+}- Mn^{3+} coupling is reported to occur at higher temperatures resulting in the fact that both Mn and Ho sublattices have same CM order below ~27 K and preserves the coherence between the Ho^{3+} and Mn^{3+} magnetic systems down to the very low temperatures [12]. For these compounds a mechanism of ferroelectric polarization, based on the exchange-striction is proposed. It is predicted that this mechanism generate a much larger ferroelectric polarization than inverse DMI [4–6]. Thus, the polarization arising from the Ho^{3+}-Mn^{3+} exchange-striction exists down to lowest temperatures of the same magnitude as that of Dy^{3+}-Mn^{3+} above the T_N^{Dy} in DMO. Therefore, the sequential substitution of Dy^{3+} by Ho^{3+} allows one to control the entire spin structure (not just the spin structure of the RE subsystem) and to adjust the multiferroicity of $RMnO_3$ by changing the RE ions [20–24]. The recent studies of substituted compounds $Dy_{1-x}Ho_xMnO_3$ demonstrate the enhancement of ferroelectric polarization at low temperatures [22], it was supposed there that complete suppression of the Dy-ordering-related polarization drop-down could be reached by the doping level of $x = 0.2$. This implies the preservation of the coherence between the R^{3+} magnetic subsystem with the Mn^{3+} spins in the cycloidal magnetic phase below the T_{NR}. Moreover, the Ho-substituted powder samples showed higher polarization in comparison to the parent pure DMO. Such a substitution seems to be a promising technological way of both the enhancement of the polarization magnitude itself, but also to extend the temperature region where the stable polarization could be exploit. The details about the magnetic order in the mixed compound DHMO remains however unstudied. Moreover, the direct correlation between the observed enhancement of the electric polarization and the preservation of the cycloidal order is still missing. In order to study the coupling between the RE and Mn magnetic subsystems in $Dy_{1-x}Ho_xMnO_3$ ($x = 0.2$) multiferroic in detail and to clear the effect of the RE ion type on the magnetic order and subsequent electric polarization, single crystal neutron diffraction experiments (including polarized neutrons diffraction) were carried out. The macroscopic measurements of electric polarization in the same sample are important point of this study in order to establish a direct link between microscopic details on the magnetic structure to the macroscopic properties.

2. Experimental

High quality single crystals of $Dy_{0.8}Ho_{0.2}MnO_3$ (DHMO) were grown by the spontaneous crystallization from a solution in a melt. The ratio of the chemical reagents $PbO:PbF_2:B_2O_3$ used as a solvent was 0.84:0.14:0.01 respectively. The ratio of the desired composition $Dy_{0.8}Ho_{0.2}MnO_3$ to the solvent was 1:9. High purity reagents 99.9% (Alfa Aesar) of PbO, PbF_2, MnO_2, Dy_2O_3, Ho_2O_3, B_2O_3 were used for synthesis. The technological regime consist of heating the charge in a platinum crucible to 1200 °C, followed by cooling for two weeks to a temperature of 700 °C. The obtained single crystals have the shape of parallelepipeds with sizes up to 1.5 × 1.5 × 3 mm^3, shiny surfaces and black color. The synthesis and characterization of the orthorhombic single crystals of the family $Dy_{1-x}Ho_xMnO_3$ (x = 0–0.4) were described in detail in our previous work [25].

For the electric polarization measurements plate-like sample in the form of a flat capacitor was prepared. The capacitor plates were formed from an epoxy-based conductive paste with a silver filler deposited onto the preliminary polished crystal faces perpendicular to the crystallographic *a*-axis. The electric polarization was determined by measuring the electric charge flowing-off the capacitor plates with a Keithley 6517 B electrometer.

Measurements of the magnetic properties were carried out at the Kirensky Institute of Physics on an in-house-made vibration magnetometer with a superconducting solenoid. This magnetometer is designed for precision measurements of magnetic characteristics of various materials using an automated measuring system. The device allows to measure the magnetization as function of temperature M(T) in the range of 4.2–300 K and in applied magnetic fields up to 6 T as M(H).

The neutron diffraction studies were performed at diffractometer POLI [26] at the Heinz Maier-Leibnitz Zentrum (MLZ, Garching). Single crystal diffractometer POLI is specialized on different methods of polarized neutron diffraction. In order to obtain quantitative chiral characteristics of magnetic structures the method of spherical neutron polarimetry (SNP) [27] was used. It allows to determine all components of the scattering polarization matrix. SNP technique is implemented on POLI using third generation zero-field Cryogenic Polarization Analysis Device CRYOPAD [28]. The unique feature of POLI is that it uses ^3He spin filters for neutron polarization and analysis. Such a setup is very efficient for the short wavelength neutrons in order to increase the angular resolution and the flux density of the polarized neutrons on the sample position. On the other side, the time dependence of the polarizing (analyzing) efficiency of the filters represents a main drawback of the technique, since the precise knowledge of the incoming and scattered beam polarization is essential for the SNP. This requires some additional corrections, which may lead to a decrease in the statistical accuracy of the measurement. The standard correction procedure described elsewhere [29] was applied to the SNP data.

Measurements of the chiral scattering in the external electric field were made in a “half polarized” mode, i.e. without analysis of the polarization for the scattered neutrons. This mode is less time consuming than SNP because it avoids the transmission of the analyzer, but still gives the possibility to measure the pure chiral scattering by *xx* components of the polarization matrix. The results of these measurements were scaled then with those from SNP data. In order to apply an electric field during measurement, the crystal was glued between two aluminum plates forming kind of electric capacitor using non-magnetic, electrically isolating ceramic screws (Fig. 1). The electric field was applied along the *c*-axis in the crystal. The sample was cooled down using dedicated long-tale top-loading closed-cycle cryostat model Janis SHI-950-T. The essentials of the measurements with high electric fields in the cryogenic environments consist in fine-tuning the pressure of helium exchange gas continuously along a thin line where it is possible to apply several kV/mm voltage on the sample without an electric breakdown maintaining the necessary temperature of the sample at the same time. A reliable setup for the in-situ pressure control and regulation within a cryostat has been developed and calibrated before the experiment was started.

In all SNP experiments we employed the coordinate system which is conventional for the studies with polarized neutrons in which the instrumental $\boldsymbol{x}$-direction coincides with the scattering vector $\boldsymbol{q}$, the $\boldsymbol{y}$-direction lies in the scattering plane and is perpendicular to $\boldsymbol{x}$, and the $\boldsymbol{z}$-axis is directed vertically forming the right-handed Cartesian system.

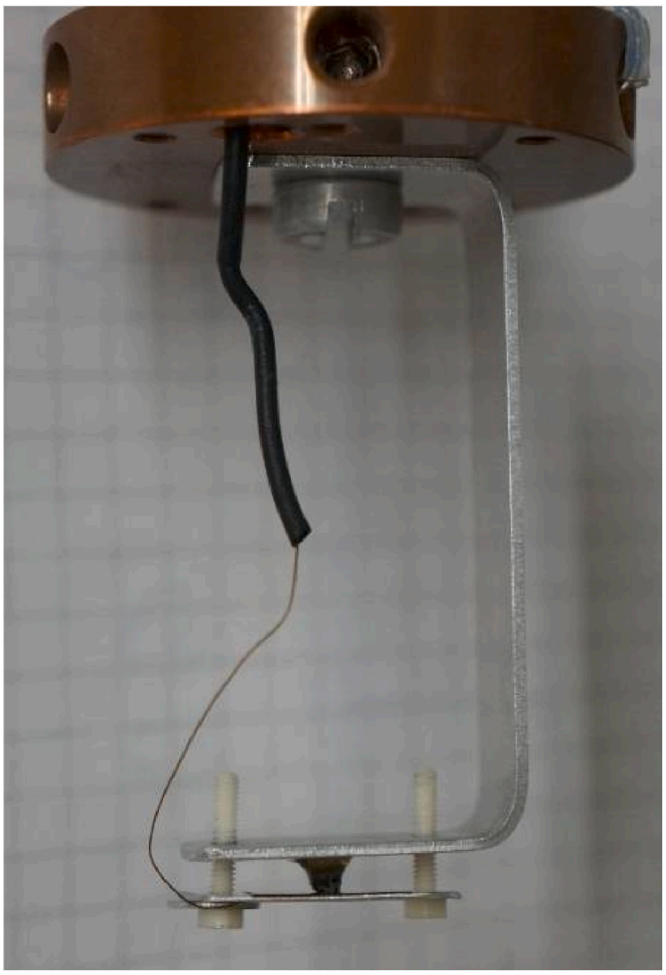

Fig. 1. $Dy_{0.8}Ho_{0.2}MnO_3$ single crystal placed between two aluminum electrodes on the cold finger of cryostat.

The crystal orientation was chosen as follows: *c*-axis was oriented vertically, *a* and *b* axes lying in a horizontal scattering plane.

3. Results and discussions

3.1. Crystal structure of $Dy_{0.8}Ho_{0.2}MnO_3$

For the crystal structure refinement of DHMO 542 nuclear Bragg reflections were measured on the single crystal diffractometer POLI at wavelength λ = 0.897 Å in non-polarized mode. Two data collections were performed: at room temperature and at 4 K respectively. Among measured data 179 independent Bragg reflections satisfying condition I > 3σ(I) were used for the structure refinement. Obtained for substituted compound DHMO results reveal that space group *Pbnm* describes well its crystal structure at both temperatures. Only reflections allowed in *Pbnm* space group were detected and no splitting within the resolution of POLI diffractometer observed. Atomic positions in DHMO resulting from the refinement at 300 and 4 K are shown in Table 1. Like it was in a case for DMO [11], no significant difference was detected in the unit cell parameters as well as in the atoms coordinates for low temperature, below T_N. As it can be seen from Table 1, the structure parameters for the both "pure" DMO and substituted DHMO are very similar. Thus, the substitution of Dy by Ho at level of 0.2 does not change the overall crystal structure. Assuming that Ho occupies the same Wyckoff position 4c as Dy and the total occupation of the RE site is one, the degree of the replacement of Dy by Ho was checked when refining the crystal structure of DHMO. The occupancies obtained as a result of structural refinement were equal 0.79 (3) for Dy and 0.21 (3) for Ho respectively, that is in the perfect agreement with the expected molar ratio from the crystal growing.

3.2. Magnetization measurements

In order to have base for the comparison, the field dependences of the magnetization both in DMO and DHMO single crystals were measured along different crystallographic directions at $T = 4.2$ K, they are shown in Fig. 2. Easy to observe, that both crystals studied in this work have a significant magnetocrystalline anisotropy demonstrating quasi easy-plane behavior. However, a significant in–plane anisotropy is also present. The magnetization measured with field along *b* axis is greater than that along *a* axis. It can be seen also from Fig. 2 that in DHMO value of the magnetization along the *c* axis is greater than that in DMO. This is also in a good agreement with the results of magnetic structure refinement from neutron data (shown at Table 3), where rare-earth magnetic moments component along *c* axis are zero for DMO and have non-zero values for DHMO. That means that a partial replacement of Dy with Ho leads to a decrease in the magnetic moment at rare earth element along both the *a* and *b* axes and induces component along *c*.

3.3. Electric polarization measurements

Spontaneous electric polarization in DMO of about 1400 μC/m^2 induced by magnetic transition to the chiral phase (at $T \sim 19$ K) is directed along the *c* axis [1–3]. An external magnetic field applied along the *a* or *b* axes leads to the switch of the electric polarization vector $\boldsymbol{P}_c \rightarrow \boldsymbol{P}_a$, that can be connected with the change of magnetic structure (flop of the Mn cycloid plane from the *bc* into *ab* crystallographic plane) [1–3, 30]. This switch process is arising in the both magnetic field orientations $\boldsymbol{H}_b$ and $\boldsymbol{H}_a$, but in the case of $\boldsymbol{H}_b$ this occurs at the smaller field values and leads to the higher polarization value $\boldsymbol{P}_a$ of more than 2000 μC/m^2. Here we present the results of the measurements of the polarization $\boldsymbol{P}_a$ only due to some limitations in the used samples geometry and expected higher absolute polarization values. Fig. 3 a and b shows the field dependences of the magnetoelectric polarization $\boldsymbol{P}_a(\boldsymbol{H}_b)$ for the crystals DMO [31] and DHMO respectively. The red curves were measured after pre-cooling the sample from 100 to 4.2 K in both electric $\boldsymbol{E}_a = 7.4$ kV/cm and magnetic $\boldsymbol{H}_b = 30$ kOe fields. Cooling in the magnetic field $\boldsymbol{H}_b$ leads

Table 1
Fractional atomic positions in DMO and DHMO at various temperatures resulted from the structure refinement in space group *Pbnm*, determined by single crystal neutron diffraction.

Atom	$DyMnO_3$, 2.4 K [11] a = 5.269 (7), b = 5.845 (4), c = 7.331 (4) Å			$Dy_{0.8}Ho_{0.2}MnO_3$, 300 K a = 5.27 (1), b = 5.840 (4), c = 7.360 (8) Å			$Dy_{0.8}Ho_{0.2}MnO_3$, 4 K a = 5.268 (3), b = 5.835 (4), c = 7.358 (1) Å		
	x	y	z	X	Y	Z	x	y	z
Dy/Ho, 4c	−0.0180 (2)	0.0829 (2)	0.25	−0.0169 (5)	0.0820 (1)	0.25	−0.0178 (4)	0.0830 (9)	0.25
Mn, 4 b	0.5	0	0	0.5	0	0	0.5	0	0
O1, 4c	0.1088 (9)	0.4622 (4)	0.25	0.1083 (3)	0.4640 (4)	0.25	0.1093 (3)	0.4622 (2)	0.25
O2, 8 d	0.7022 (5)	0.3276 (5)	0.0527 (6)	0.7020 (4)	0.3285 (5)	0.0513 (6)	0.7013 (9)	0.3272 (4)	0.0525 (5)
				$R_F = 1.94$			$R_F = 1.51$		

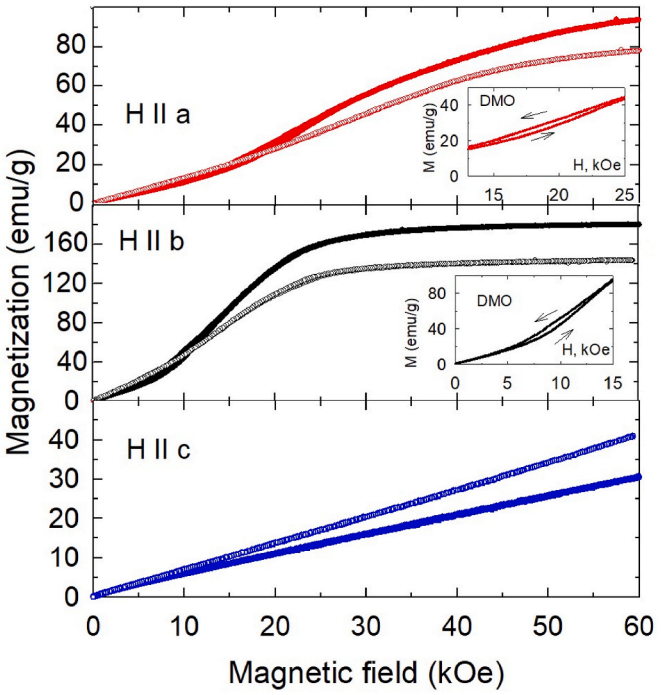

Fig. 2. Field dependences of the magnetization in single crystals of DMO (closed circles) and, DHMO (open circles) respectively measured along main crystallographic directions at T = 4.2 K. Insets: hysteresis portions of DMO curves on an enlarged scale. Arrows show the variation in the external field direction.

to a reorientation of the vector of spontaneous polarization $\boldsymbol{P}_c \rightarrow \boldsymbol{P}_a$ [1–3, 31]. The electric field $\boldsymbol{E}_a$ was applied to ensure that the resulting ferroelectric state $\boldsymbol{P}_a$ is single domain one. After reaching the temperature of liquid helium, the poling voltage was switched-off and the measurement process starts. For both compounds, the polarization obtained after this prehistory reaches large values of $\boldsymbol{P}_a$2200 and ~1600 μC/m^2 for the pure and substituted samples, respectively. This is in a perfect agreement to the previously reported values for DMO from the single crystal measurements [3]. When the magnetic field is decreased down to $\boldsymbol{H}_b$ ~17 kOe in DMO and to $\boldsymbol{H}_b$ ~20 kOe in DHMO, a sharp drop in polarization occurs, which is associated with the re-switching of the polarization direction $\boldsymbol{P}_a \rightarrow \boldsymbol{P}_c$ (the course of the curves is indicated by the number 1 in Fig. 3 (a, b)). The following switching $\boldsymbol{P}_c \rightarrow \boldsymbol{P}_a$ occurs again by the magnetic field increasing above $\boldsymbol{H}_b$ ~20 kOe with some coercive field hysteresis of about 1.5–2 kOe. Whereat, the coercive field strength in the substituted sample is smaller than in the DMO. This observation on the ferroelectric domains somehow correlates to the observed hysteresis loops with similar coercivity in the magnetization behavior of pure DMO (inset to Fig. 2) and less pronounced magnetization hysteresis for the DHMO sample, denoting strong coupling between the magnetic and ferroelectric domains (multiferroic domains [32,33]).

After repeated field increase, the polarization $\boldsymbol{P}_a$ does not reach the previous values (curves 2). We attribute this behavior to the absence of a poling electric field $\boldsymbol{E}_a$. With each subsequent iteration, the resulting $\boldsymbol{P}_a$ polarization decreases, and the crystal begins to "forget" the preferred $\boldsymbol{P}_a$ direction originally set by the external electric field, i.e. a domains with the different direction of the polarization tends to an equilibrium. This behavior is similar for both pristine and substituted compounds. The black curves [in Fig. 3 (a, b)] correspond to polarization measured after cooling the sample in an electric field $\boldsymbol{E}_a$ = 7.4 kV/cm without applying an external magnetic field. In this case, when a magnetic field $\boldsymbol{H}_b$ is applied, the sample, that initially has spontaneous $\boldsymbol{P}_c$ polarization also experiences $\boldsymbol{P}_c \rightarrow \boldsymbol{P}_a$ transition. Small increase of $\boldsymbol{P}_a$ is observed at about 10 kOe in both samples, whereas here DHMO has slightly higher values. In the region of ~20 kOe different behavior was observed for two compounds: in DMO sample $\boldsymbol{P}_a$ further increase with field, while in the DHMO sample polarization lowering could be accounted. During this transition, the external electric field $\boldsymbol{E}_a$ is already removed and the sample enters the multi-domain state $\boldsymbol{P}_a$, in which domains with polarization directed along $+a$ and $-a$ do exist. This results in a compensation for the macroscopic polarization of $\boldsymbol{P}_a$, and the sample demonstrates overall lower polarization. Our results show, that in the substituted sample frustrated RE magnetic ordering reacts much more flexible on the external disturbing field, than the "more rigid" well established Dy

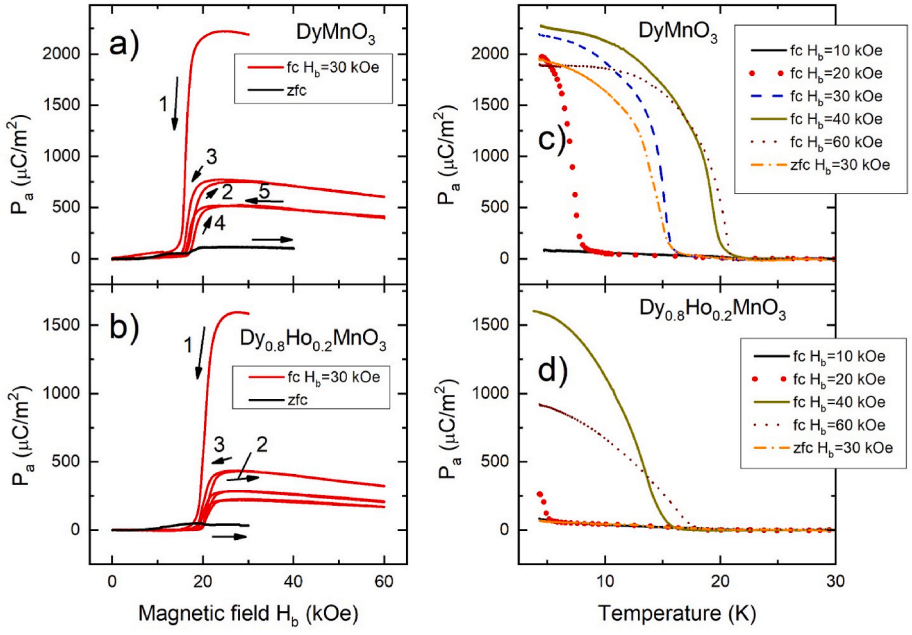

Fig. 3. Magnetic field induced electric polarization along the a axis P_a in DMO [31] a) and DHMO b) measured at 4.2 K respectively. The direction of magnetic field variation during the measurements is marked by the numbered arrows, in the correspondence with the sequence of the measurements. Temperature dependences of P_a at various magnetic fields for DMO [31] c) and DHMO d).

ordering in pristine DMO in good agreement with the proposed from the neutron diffraction [11] scenario of "Dy-controlled" and "Mn-controlled" magnetic states. This assumption fits well to the observed smaller hysteresis in DHMO. Previously published results on Ho substitution in $Dy_{1-x}Ho_xMnO_3$ powders have shown overall polarization increase with increasing level of substitution between $x = 0 \div 0.3$ from about 250 to 550 μC/m^2 at low temperature (2 K) and zero applied field [22]. From the comparison of the red curves in Fig. 3 (a, b), it is seen however, that the polarization $\boldsymbol{P}_a$ in DMO is indeed larger comparing to that one in substituted DHMO. It is worth noting that it is hardly possible to directly compare the overall spontaneous polarization in zero field from the powder sample with the field-induced polarization along a certain direction in the single crystal. As shown in Ref. [22] the application of the magnetic field of 30 kOe reduces the accounted polarization in the x = 0.1 DHMO powder sample almost double from about 400 to 200 μC/m^2. In our case, such a field strength is just necessary to create much larger $\boldsymbol{P}_a$ in the single crystal. So, a direct comparison between our results from the pristine and substituted single crystals do not confirms the previously reported absolute polarization value enhancement due to the Ho substitution.

The noticeable differences in the behavior of ferroelectric polarization of DMO and DHMO are observed at the temperature dependences (Fig. 3 (c) and (d), respectively). Measurements of temperature dependencies were made in the heating mode after cooling with the simultaneously applied electric $\boldsymbol{E}_a$ and magnetic $\boldsymbol{H}_b$ fields, as described above, except for the zfc curves shown in orange in Fig. 3 (c, d), which will be discussed later. As shown in Fig. 3 (c and d), after cooling in the $\boldsymbol{H}_b = 10$ kOe, the polarization $\boldsymbol{P}_a$ increases only slightly reaching similarly large values for both samples. This field is not sufficient to induce the polarization flop of $\boldsymbol{P}_c \rightarrow \boldsymbol{P}_a$. In the 20 kOe field-cooled samples the $\boldsymbol{P}_a$ reaches significant values in DMO, transition happening at about 7 K. In DHMO however, only the beginning of the $\boldsymbol{P}_c \rightarrow \boldsymbol{P}_a$ transition is induced by $\boldsymbol{H}_b = 20$ kOe at $T = 4.2$ K (Fig. 3 (d)). The shift of 3–4 K towards lower temperatures is observed. As the temperature increases, the polarization undergoes reverse transition $\boldsymbol{P}_a \rightarrow \boldsymbol{P}_c$ after which the curve of polarization dependence coincides with the curve measured in $\boldsymbol{H}_b = 10$ kOe. A further increase of the magnetic field leads to a shift of the $\boldsymbol{P}_a \rightarrow \boldsymbol{P}_c$ transition towards higher temperatures up to the transition temperature T_{Ch} ~20 K for DMO and about 16 K for DHMO respectively, still maintaining the observed low temperature shift of about 4 K. This value is in a good agreement to that determined from the thermal evolution of the magnetic structure by the neutron diffraction and polarization analysis. For the DMO, the ferroelectric state is more stable and continues to exist in larger magnetic fields up to temperatures even exceeding temperature of the magnetic transition T_{Ch} defined in the absence of a magnetic field. One should also mention the curves shown in orange in Fig. 3 c and d. They were measured after cooling in zero magnetic and electric fields down to a temperature of 4.2 K, after which a constant poling field $\boldsymbol{E}_a$ and an external magnetic field $\boldsymbol{H}_b = 30$ kOe were applied to the samples. After that, the electric field was removed, and measurements of temperature dependences of $\boldsymbol{P}_a$ were made while heating. As shown in Fig. 3 (c) after this prehistory, the polarization in the DMO is quite large and almost reaches the values obtained after cooling in the field. A completely different picture is observed for the substituted sample DHMO. For that crystal, the polarization obtained after such a prehistory does not differ from the polarization in the 10 kOe field, which indicates that the $\boldsymbol{P}_c \rightarrow \boldsymbol{P}_a$ transition is not induced. This means that also no flop of the Mn cycloidal magnetic order plane is produced in the DHMO, denoting that Ho substitution leads not only to some frustration of magnetic order on the RE position, but also directly influences on the Mn magnetic sublattice as well, e.g. by strengthening the RE-Mn interactions.

3.4. Temperature evolution of the magnetic structure

The studies of the thermal evolution of the magnetic structure of $Dy_{0.8}Ho_{0.2}MnO_3$ sample were performed on the polarized neutron diffractometer POLI with the short neutron wavelength λ = 0.897 Å in non-polarized mode. It was observed that the magnetic ordering in $Dy_{0.8}Ho_{0.2}MnO_3$ takes place at same temperature T_N^{Mn} ~38 K like in $DyMnO_3$, with the similar propagation vector $\boldsymbol{k}^{Mn} = (0\ k_y\ 0)$ and slightly higher initial propagation vector component $k_y = 0.367$ (2). It is convenient to trace it via the temperature dependence of the satellite (2 k_y 1) (Fig. 4). The intensity of this magnetic satellite increases gradually below T_N^{Mn} down to about 26 K, below which it remains constant until the crossover point ~16 K (note it coincides with T_{CE} for DHMO). Below that temperature the intensity starts increase much faster while cooling. This behavior is similar to that observed in DMO sample below 19 K due to the induced RE ordering, just happening at slightly lower temperature ($\Delta T \sim 3$ K). The absence of the significant intensity hysteresis between the heating and cooling mode in DHMO, as well as no sharp change in the intensity of the satellite down to 4 K (lowest temperature available within POLI cryostat) [Fig. 4(a)], indicates that during our experiment in DHMO sample we always remained in the "Mn-controlled" state (in the terms of ref. [11]). Neither thermal evolution of the wave vector, no that of the FWHM in DHMO show thermal hysteresis below 16 K, demonstrating reversible thermal effect on the magnetic structure in the state where RE is mostly polarized by Mn. Above 16 K, however, the propagation vector shows a significant hysteresis between cooling and heating modes. Wave vector component k_y keeps constant value of 0.367 (3) while cooling from 38 K down to ~ 26 K. Below this temperature, k_y increases rapidly and becomes equal to 0.382 (2) at $T_{Ch} \approx 16$ K and then it remains constant. One can suppose that this temperature T_{Ch} corresponds to the transition from non-chiral spin wave type structure to

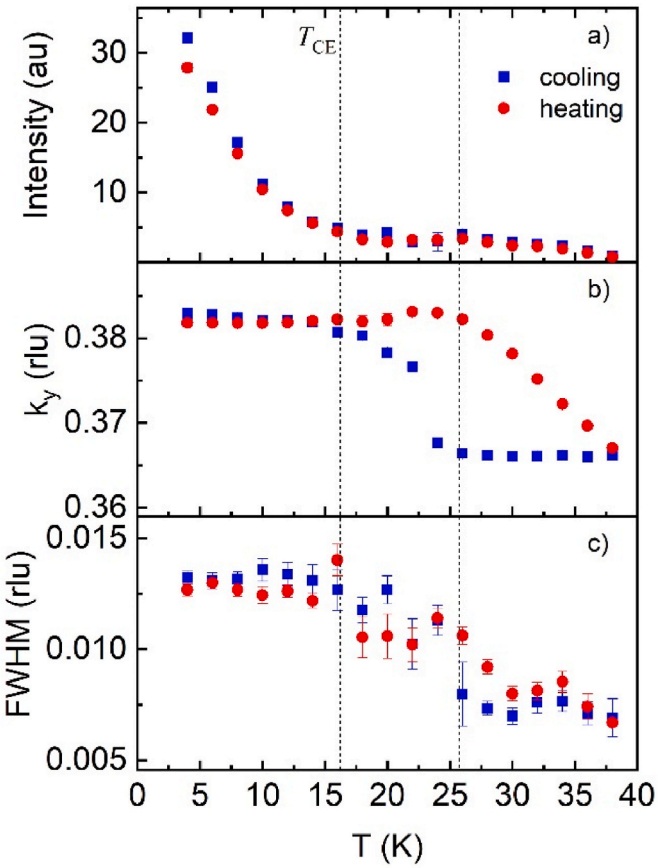

Fig. 4. Temperature evolution of the ICM magnetic Bragg reflection (2 k_y 1) in $Dy_{0.8}Ho_{0.2}MnO_3$ samples respectively by cooling and heating: a) the integrated intensity; b) the wave vector evolution; c) full widths at half maximum (FWHM) of the magnetic peaks. The vertical broken lines indicate the observed characteristic magnetic phase transition temperatures.

cycloid, which is chiral. In the heating mode, however k_y does not change its value up to ~26 K, then gradually decreases to the initial value $k_y = 0.367$ (3) [Fig. 4(b)]. The observed two special temperature points: 26 K and 16 K are well corresponding to the trend-change temperature

Points from the intensities graph (Fig. 4(a)) and those of peak width (Fig. 4(c)). At the same time, the temperature dependence of the satellite peak-width does not show any noticeable hysteresis. Nonetheless, it is worth noting that the FWHM increases (almost doubling) between 26 K and 16 K. We relate these features to the strong interaction of the two magnetic systems – manganese and rare earth ones.

The orbit of the manganese ions in the unit cell corresponds to position 4 b with sufficiently high-symmetric coordinates: Mn1 (½ 0 0), Mn2 (½ 0 ½), Mn3 (0 ½ ½), Mn4 (0 ½ 0). This gives the opportunity to obtain a correspondence between the parity type of Miller indices of the Bragg peaks and magnetic Bertaut modes [34] for the manganese subsystem, as it was done in work [15]. This means, that to the reflections of type h + k – even, l – odd only A-mode, and to the reflections of type h + k – odd, l – even only C-mode, to those with h + k – even, l – even – only F-mode, and to those with h + k – odd, l – odd – only the G-mode will give a contribution. This is not quite precise for the incommensurate magnetic wave vector $\boldsymbol{k}_{Mn} = (0\ k_y\ 0)$, but nevertheless permits to make some meaningful estimations. Just below $T_N \approx 38$ K satellites of type A emerge, originating from manganese ordering (Fig. 5), i.e. only the manganese magnetic subsystem contributes to these peaks. At T ~32 K the satellites of type F appear, signifying the additional contribution to the magnetic ordering, which is also similar to situation at DMO [35]. Thus, it is reasonable to assume that these satellites originated from the weakly polarized rare earth subsystem. At T ~16 K a new set of satellites corresponding to type C (h + k – odd, l – even) emerges and their intensities increases rapidly (Fig. 5). That is polarization effect from Mn sublattice produces some changes in RE one below 16 K, leading to the emergence and increase of new type of reflections.

3.5. Spherical neutron polarimetry

The SNP measurements on DHMO were performed in order to distinguish between different possible magnetic structure models and to have some quantitative reference point for the estimation of the chiral scattering. Experiments with SNP technique were performed on the diffractometer POLI with neutron wavelength λ = 0.897 Å. Polarization matrix elements are determined as

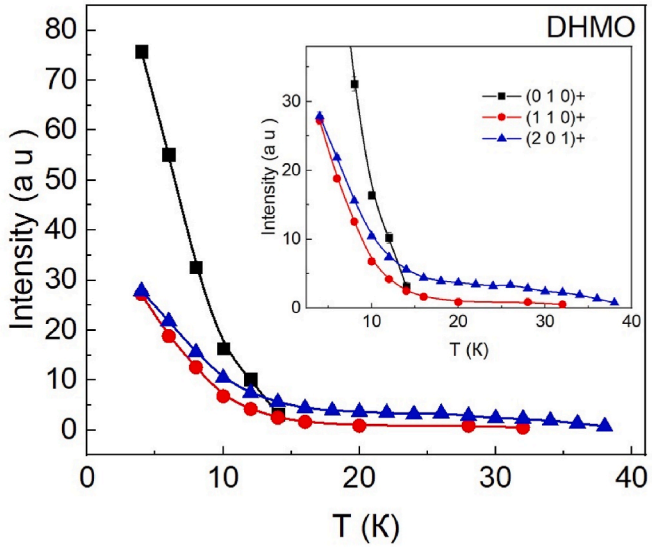

Fig. 5. Temperature evolution of the magnetic satellites of different parity (as defined in the main text) in $Dy_{0.8}Ho_{0.2}MnO_3$.

$$P_{ij} = \left(I_{ij}^{+} - I_{ij}^{-}\right) \Big/ \left(I_{ij}^{+} + I_{ij}^{-}\right) \quad (1)$$

where *i*, *j* – directions of the initial and final polarization, I_{ij}^{+} - intensity, measured after the scattering with final polarization along *j*, I_{ij}^{-} - intensity, measured after the scattering with final polarization opposite to *j*. The full polarization matrices for a number of magnetic satellites of different type were measured in DHMO at 4 K. Table 2 shows the results for satellites (2 0.382 1) and (1 1.382 0) respectively. For the magnetic satellite of A-type (2 0.382 1), the elements of the polarization matrix P_{yy} and P_{-zz} are close to 1, while elements P_{-yy} and P_{zz} are close to −1. These elements could be expressed as [27]:

$$P_{yy} = P_{-zz} = -P_{zz} = -P_{-yy} = \left(M_y M_y^* - M_z M_z^*\right) \Big/ \left(M_y M_y^* + M_z M_z^*\right) \quad (2)$$

where M_y, M_z – components of the effective magnetic interaction vector $\boldsymbol{M}_\perp = (\boldsymbol{e} \times \boldsymbol{F}_M \times \boldsymbol{e})$, with $\boldsymbol{e}$ – scattering vector, $\boldsymbol{F}_M$ – magnetic structure factor.

This unambiguously proves that the z component of the magnetic moment is very small (if any), so basically the moment is pointing along *y* direction, which is close to the crystal axis *b* for this particular reflection where mostly the magnetic moment of the Mn^{3+} positions contributes.

The diagonal components of the polarization matrix for the F-type magnetic satellite (1 1.382 0) P_{yy}, P_{-zz}, P_{-yy} and P_{zz} have small absolute values (see Table 2). While non-diagonal elements P_{zy}, P_{-zy}, P_{-yz} are close to −1 or to 1. These elements can be expressed in the following way [27]:

$$P_{zy} = P_{yz} = -P_{-zy} = -P_{-yz} = 2Re(M_y M_z^*) \big/ \boldsymbol{M}_\perp \boldsymbol{M}_\perp^* \quad (3)$$

Inspecting the experimental values related to the expressions (2) and (3) for the reflection (1 1.382 0) lead us to the conclusion that there should be a non-zero magnetic moment along the *z*-axis. For the scattering geometry of the satellite (1 1.382 0) the *z*-axis corresponds exactly to the crystallographic *c*-axis. Since F-type reflections originate from the RE magnetic sublattice, this statement refers to the magnetic moments of Dy^{3+}/Ho^{3+} ions.

The chiral non-diagonal terms P_{yx}, P_{zx}, P_{-yx} and P_{-zx} of all matrices are equal to 0 within the measurement error. In this case, one can assume that the structure is either not chiral or it has an equal population of right and left-handed chiral domains. We assume that the latter is applicable in our case and the reasoning for that will follow in the next sections.

Table 2
Measured polarization matrices for magnetic satellites (2 0.382 1) and (1 1.382 0) at 4 K in DHMO.

		(2 0.382 1)			*(1 1.382 0)*		
		Pout			*Pout*		
		X	y	z	x	Y	z
Pin	X	−0.98 (5)	0.16 (6)	0.12 (6)	−0.95 (6)	0.12 (8)	0.01 (7)
	Y	−0.01 (5)	0.91 (5)	−0.06 (6)	0.02 (6)	0.30 (5)	−0.62 (8)
	Z	0.05 (5)	−0.09 (5)	−0.90 (7)	0.01 (5)	−1.0 (1)	−0.26 (7)
Pin	-x	0.98 (5)	0.01 (5)	0.03 (5)	0.95 (6)	−0.08 (7)	0.01 (7)
	-y	−0.00 (5)	−0.92 (4)	0.07 (5)	−0.08 (6)	−0.28 (5)	0.98 (9)
	-z	−0.04 (4)	0.05 (5)	1.04 (8)	0.02 (6)	0.81 (9)	0.31 (7)

Table 3
Magnetic structures of DMO [11] and DHMO.

	Temperature	Magnetic moment	Wave vector	Mode	M_x, μ_B	M_y, μ_B	M_z, μ_B
DMO	2.4 K	Mn	(0 k_y 0)	A_yA_z	0	2.92 (26)	2.77 (21)
		Dy	(0 k_y 0)	G_xA_y	2.49 (8)	5.57 (7)	0
		Dy (CM)	(0 0.5 0)	G_xA_y	3.51 (1)	6.62 (6)	0
DHMO	4 K	Mn	(0 k_y 0)	A_yA_z	0	3.471 (15)	0.147 (13)
		Dy	(0 k_y 0)	$G_xA_yA_z$	1.922 (15)	4.531 (15)	0.950 (11)
		Ho	(0 k_y 0)	$G_xA_yA_z$	4.786 (15)	7.141 (14)	4.173 (12)

3.6. Refinement of magnetic structure from single crystal neutron diffraction data $Dy_{0.8}Ho_{0.2}MnO_3$

The data set for the refinement of the magnetic structure in DHMO was measured on diffractometer POLI with wavelength λ = 0.897 Å in non-polarized mode using lifting counter. About 150 reflections, corresponding to incommensurate propagation vector $\boldsymbol{k}_{Mn}$ = (0 0.38 0) were collected at 4 K. Since the crystal structure of DHMO found to be the same as in DMO, therefore the representation analysis made for DMO can also be applied to DHMO. The refinement then was performed with FullProf suite [36]. In the same way as for DMO [11] we used the same model of elliptical spin cycloid for the refinement of magnetic structure in DHMO sample. However, the magnetization measurements (Chapter 3.2) and SNP results (one should pay attention on the consideration of polarization matrix elements of (1 1.38 0) satellite in Chapter 3.5) show the existence of *c*-component of the magnetic moment in the RE system. Thus Mn magnetic order of A_yA_z configuration and RE order of $G_xA_yA_z$ one give satisfactory fit with $\chi^2 = 2.83$ in contrast to $\chi^2 = 7.11$ resulting from RE configuration of G_xA_y, i.e. without *c*-component. The refined magnetic moments values are: $\boldsymbol{M}_{Mn}$ = (0, 3.471(15), 0.147(13)) μ_B, $\boldsymbol{M}_{Dy}$ = (1.922(15), 4.531(15), 0.950(11)) μ_B, $\boldsymbol{M}_{Ho}$ = (4.786(15), 7.141(14), 4.173(12)) μ_B (see Table 3). Thus, the refinement of DHMO magnetic structure shows that it is of elliptical type with strong ellipticity – that is, it is of chiral type. Comparing to DMO at 2.4 K [11], *b*-component of the magnetic moment on Mn ion is a little larger, while *c*-component is significantly reduced in DHMO. The lower value of ordered *c*-component of Mn magnetic moment can be attributed to the impact of Ho doping in RE subsystem, the disturbing influence of which increases with temperature decrease, as it can be judged by gradual increase of the satellite width [Fig. 4(c)]. Magnetic moments of the Dy ions have value a little lower than that obtained for DMO at low temperatures [11]. The value of Ho moment in DHMO (8.27 μ_B) is slightly higher than those ones reported in the literature for pure $HoMnO_3$: 7.27 μ_B [12], 7.7 μ_B [8] and is closer to free ion value of 10 μ_B.

3.7. Measurement of chiral scattering under applied electric fields in DHMO

Polarized neutron diffraction without polarization analysis was used in order to trace the magnetoelectric coupling in the DHMO multiferroic phase. The measurements of chiral scattering dependence from the external electric field were performed with applied voltage up to +7.5 kV (i.e. field ~24.2 kV/cm) at temperatures 16 K–20 K (close to the T_{CE} in DHMO). This electric field value corresponds to the maximum reachable on the sample with a positive polarity without an electric breakdown. Only −2.5 kV could be applied in the opposite polarity resulting in some field "asymmetry" in the experimental setup.

The chiral scattering was measured without polarization analysis after scattering by the sample. Initial neutron polarization was directed along the scattering vector and could be flipped – thus the magnetic scattering intensities I_x^+ and I_x^- were measured. The difference of these intensities yields the chiral scattering:

$$I_x^+ = I_M + I_{Ch}, I_x^- = I_M - I_{Ch} \quad (4)$$

$$2I_{Ch} = I_x^+ - I_x^- \quad (5)$$

Where I_{Ch} - the chiral contribution to the scattering. Using this method the measurements of the magnetic chirality as function of applied electric field were performed on the satellite (2 0 1)$^+$. Small, but clearly visible difference $I_x^+ - I_x^-$ could be identified at 16 K in heating mode even with zero electric field [Fig. 6]. This observation may serve as a direct confirmation to the fact, that the magnetic structure in DHMO at 16 K is of the chiral type and some slight imbalance between the right- and left-handedness chiral domains exists in the sample at this temperature. The weakness of the chiral scattering also could be attributed to the fact that magnetic envelope has strong ellipticity, which is close to the achiral collinear structure.

The field measurements were performed with the external electric field applied along the crystal *c* axis and the scattering asymmetry was calculated as

$$A = \left(I_x^+ - I_x^-\right) / \left(I_x^+ + I_x^-\right) \quad (6)$$

representing so-called "chiral ratio", denoting the ratio of the chiral scattering to the total magnetic scattering. The measurements were made in the heating mode, each time the temperature increase was made at the maximum positive field +7.5 kV. Then, after the temperature stabilization, the measurements were performed with decreasing field down to −2 kV. After that, the field was raised again to the maximum positive value to create a close field loop and then a new temperature was established. Fig. 7 displays the results of the measurements at different temperatures. It can be seen that the maximum chiral ratio value with negative sign is observed at 16 K (Fig. 7). It does not change its overall sign when changing the field, but kind of hysteretic behavior can be interpreted to the data in dependence on the field direction change. This means that on the one side, the mobility of the chiral domains is restricted, but on the other side the magnetic chirality can be

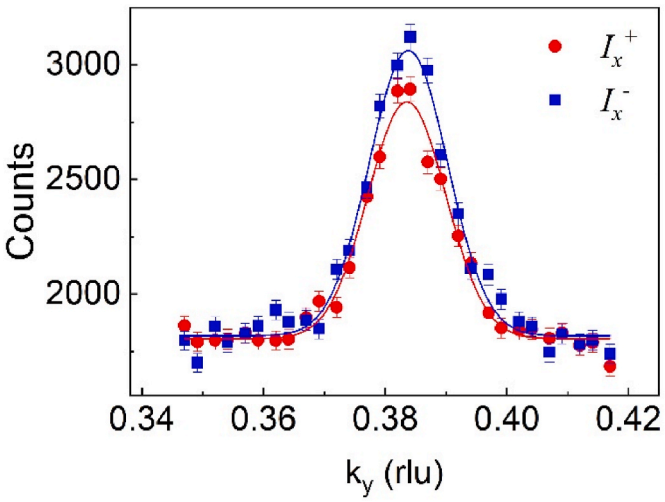

Fig. 6. Q-scans of magnetic satellite (2 0 1)$^+$ in DHMO sample performed with neutron polarization along scattering vector (I_x^+) and opposite to it (I_x^-) at 16 K and zero electric field.

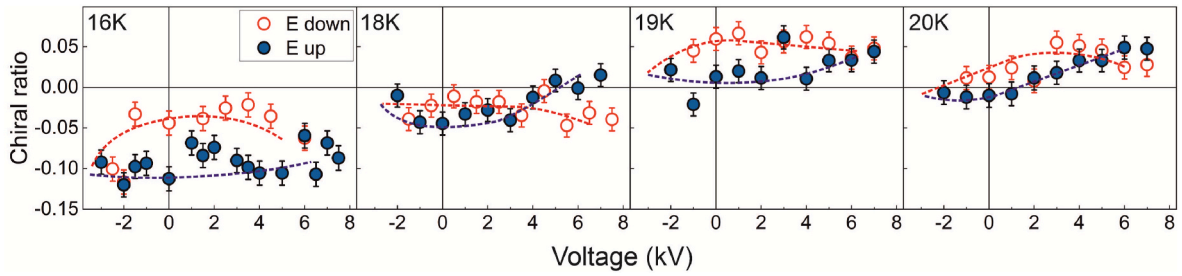

Fig. 7. The chiral scattering dependence on the external electric field in DHMO sample at temperatures between 16 K and 20 K.

significantly changed by an external electric field at the fixed temperature depending on the field history. By the heating to 18 K the average asymmetry is dropped by a half, losing its directional hysteresis, while still remaining negative. At the higher temperatures: 19 K and 20 K it changes the sign becoming slightly positive and having rather the same values at both 19 and 20 K respectively. The field dependence of the asymmetry at these temperatures has only a weak hysteretic nature (if any), which could be connected with chiral fluctuations. One can suppose that average chirality goes from negative to slightly positive because of specific way of measurements, when the measurements at each temperature were ended at the highest positive voltage, then temperature raised at this highest voltage. Thus, the measurements of the chiral scattering with polarized neutrons confirms that phase transition mentioned above in the chapter 3.4 at about 16 K in DHMO should be related to the formation of the chiral (cycloidal) magnetic order on Mn. As results from the refinement of the magnetic moment on the Mn in the chapter 3.6 this cycloid is strongly elliptic at 4 K.

The reverse of the electric field along the *c* axis favors the formation of the domain with opposite chirality (rotation direction of the spins in the cycloid) over the inverse DMI mechanism. The direct influence of the electric field on the magnetic chirality in single crystals of $TbMnO_3$ was observed by the polarized neutron scattering [32,37] and polarized light techniques (second harmonic generation) [33]. It was possible to switch between the two magnetic chiral domain populations by cooling the sample in an external electric field over the transition temperature [32] or even by varying the external field at constant temperature. The latter however, only at temperatures sufficiently close to the ferroelectric transition temperature T_{CE} [32]. By further cooling the coercive field increases significantly denoting invers dependence on the temperature. The observed hysteresis loops of the chiral scattering dependence from electric field resembles very close the field dependence of the electric polarization by the low frequency switching. Both the polarization and chiral ratio however, do not increase significantly with temperature decrease, reaching certain saturation limit just 3–4 K below the $\boldsymbol{T}_{CE}$. This denotes the strong pinning of the chiral domains and thus, reduced influence of the Mn–Mn DMI induced polarization at the lower temperatures. Principally similar behavior was observed also for the DMO single crystals [38]. Here however much smaller chiral ratios could be accounted and the hysteresis loop is much more flat resembling well the behavior of the electric polarization at zero magnetic field in this compound. The switching between different chiralities with moderate electric fields of few kV/cm is hardly possible (only within about 1 K close to the T_{CE} of about 20 K). This shows much stronger coupling between Mn and RE magnetic sublattices in DMO comparing to the $TbMnO_3$ and the importance of the exchange-striction mechanism in the occurring of the high electric polarization under applied magnetic field in the DMO. Our results on electric field dependence (in Fig. 7) for DHMO at 16 K are very similar to those observed for DMO at 18 K [38]. This denotes that Ho substitution at the level of about 20% on Dy position further increases the RE influence on the Mn sublattice confirming the initial hypothesis, that Ho doping controls not only the RE magnetic ordering solely, but the entire spin structure of the compound. The impossibility to switch the chirality sign in the DHMO sample at 16 K on the one side could be interpreted by the increased requested coercive field due to the Ho doping compared to the pristine DMO. On the other side also used here asymmetric field of −8.1/+ 24.2 kV/cm may have been insufficiently high especially at the negative value. The former polarization studies on the pure DMO [39] shows the hysteresis loops of $\boldsymbol{P}_c$ with coercive fields from 26 kV/cm up to 40 kV/cm in the temperature range 18.8 K–15.8 K respectively. In our studies, the highest electric field we could achieve in the positive polarity was of E ~24.2 kV/cm is close to the reported 26 kV/cm. Even if this can't be considered as an evident prove that Ho doping increases the coercive field, it can serve as a cross check that it is definitely not decreasing due to the Ho substitution.

In order to prove whether magnetic chirality changes with temperature, sample was cooled from 45 to 4 K ones with poling voltage of +1.5 kV and ones with opposite poling voltage of −1.5 kV. I_x^+ and I_x^- scattering intensities were measured at certain temperatures and the difference $I_x^+ - I_x^-$, denoting magnetic chirality, is built. Fig. 8 shows the measured thermal evolution. The measured chiral signal is indeed very small (at the level of the experimental standard deviation uncertainty), therefore it would be not reliable to conclude about the absolute chirality value. However, considering the data evolution clear systematics could be observed. At the temperatures above certain value T_{Ch}, the chiral scattering is very close to zero and seems to be independent on the poling voltage polarity. Below this value of about 17 K the chiral scattering increase with temperature decrease and have opposite sign for the two opposite polarities of the poling voltage. This observation clearly proves that reported previously for pure $TbMnO_3$ [32] and DMO [38], as well as for other multiferroics of type II [19,40], control of magnetic chirality by external electric field is present also in Ho doped DHMO

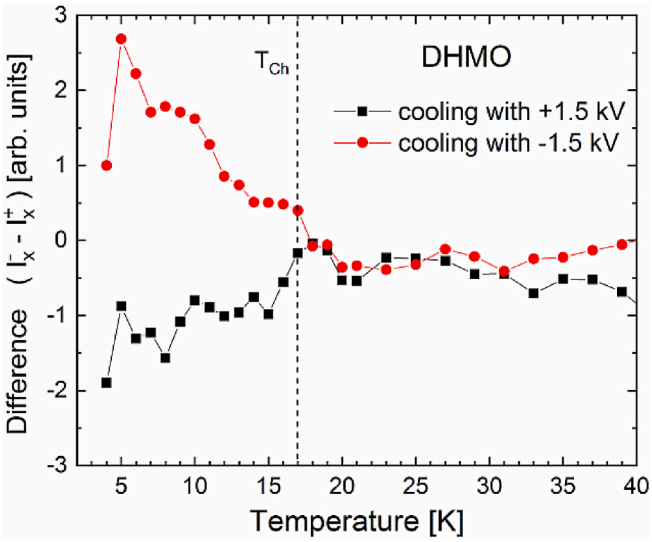

Fig. 8. The thermal dependence of the chiral scattering in DHMO sample by cooling with poling voltage of different polarity. The experimental error bars of about 2.8 arb. units are not shown for clarity.

samples.

4. Summary and conclusions

The comprehensive study of the single crystal multiferroic $Dy_{0.8}Ho_{0.2}MnO_3$ was performed by the different neutron and macroscopic methods. SNP measurements and complete polarization matrices for incommensurate magnetic structure in DHMO are reported for the first time. It was shown that $Dy_{0.8}Ho_{0.2}MnO_3$ has the same crystal structure as parent compound $DyMnO_3$ within *Pbnm* space group both at room and low temperatures (4 K) and the lattice parameters were obtained to be very similar for both compounds. No significant magnetic-order-related symmetry change was observed at low temperature within accuracy of the measurements. In the same time doping by 20% of Ho significantly changes the magnetic structure, introducing some disorder in the RE sublattice. Detailed investigation of the temperature evolution of the magnetic structure in DHMO both in cooling and heating modes confirms the existence of strong magneto-crystalline coupling but also magnetic RE-Mn coupling. Temperature hysteresis observed in DHMO differs from that one in DMO, indicating weaker influence of the RE magnetic subsystem on Mn in the substituted compound.

In the Ho doped DHMO, strongly elliptical envelope of the Mn order (almost collinear along crystal *b* direction) is observed at 4 K. This feature leads to the situation when chiral character of the magnetic order of Mn in DHMO is very weak. But using polarized neutron diffraction its appearance below 17 K could be unambiguously shown. These measurements provide an important hint for the magnetic structure model in DHMO, as they evidence the presence of RE-magnetic moment component along *c* direction, which is not the case for the undoped DMO. Thus, doping by 20% Ho on Dy position transforms RE magnetic subsystem from 2-components character to the 3-components type. That in turn leads to situation when two magnetic subsystems, manganese and rare earth ones have a coherent incommensurate spatial propagation. Resulting magnetic structure is favorable for the generating ferroelectric polarization originating from both inverse DMI at Mn subsystem and RE-Mn exchange striction mechanisms in whole temperature region of cycloidal ordering. This is the reason of the increase in the electric polarization at low temperatures reported previously in powder substituted samples [22,41].

Our ferroelectric polarization measurements on the DHMO single crystals do not demonstrate increase in the polarization value due to the Ho substitution reported for powder samples. At this point we would like to mention that it is hardly possible to make direct comparison of the overall spontaneous polarization from the powder with the field-induced polarization along an unfovarable direction in the single crystal.

By the application of electric field along *c* axis, we could change the population of the chiral domains in DHMO to a some small extent at constant fixed temperature in the vicinity of T_{Ch}. This indicates a rather strong pinning of the chiral domains to the crystal frame. Our results on electric field dependence for DHMO at 16 K are very similar to those observed for DMO at 18 K [38]. This denotes that Ho substitution at the level of about 20% on Dy position further increase the RE influence on the Mn sublattice confirming the initial hypothesis, that Ho doping controls not only the RE magnetic ordering solely, but the entire spin structure of the compound.

Credit author statement

A. N. Matveeva – Conceptualization, Methodology, Formal analysis, Data Curation, Writing - Original Draft, Writing - Review & Editing, Visualization, Investigation. **I. A. Zobkalo** – Conceptualization, Methodology, Validation, Data Curation, Writing - Review & Editing, Supervision, Project administration, Funding acquisition, Investigation, **A. Sazonov** – Investigation, Formal analysis, **A.L. Freidman** - Resources, S. V. Semenov – Resources, **M.I. Kolkov** - Resources, **K. Yu. K. Terentjev** - Resources, **N. S. Pavlovskiy** – Resources, **K. A. Shaykhutdinov** - Resources, **V. Hutanu** – Investigation, Writing - Review & Editing.

Declaration of competing interest

The authors declare the following financial interests/personal relationships which may be considered as potential competing interests: I. A. Zobkalo reports financial support was provided by Russian Foundation for Basic Research. V. Hutanu reports financial support was provided by German Research Foundation. K. A. Shaykhutdinov reports financial support was provided by Russian Foundation for Basic Research.

Data availability

Data will be made available on request.

Acknowledgments

The authors are grateful to D.A. Balaev for fruitful discussions and crystal growth management. This work was supported by the Russian Foundation for Basic Research grant # 19-52-12047, and DFG grant # SA3688/1-1, also by Russian Foundation for Basic Research, Government of Krasnoyarsk Territory, Krasnoyarsk Regional Fund of Science to the research projects number 18-42-243024 and 20-42-243008. The neutron data were obtained at the instrument POLI operated jointly by RWTH Aachen University and Jülich Centre for Neutron Science within JARA cooperation.

References

[1] T. Kimura, T. Goto, H. Shintani, K. Ishizaka, T. Arima, Y. Tokura, Magnetic control of ferroelectric polarization, Nature 426 (2003) 55, https://doi.org/10.1038/nature02018.
[2] T. Goto, T. Kimura, G. Lawes, A. Ramirez, Y. Tokura, Ferroelectricity and giant magnetocapacitance in perovskite rare-earth manganites, Phys. Rev. Lett. 92 (2004), 257201, https://doi.org/10.1103/PhysRevLett.92.257201.
[3] T. Kimura, G. Lawes, T. Goto, Y. Tokura, A.P. Ramirez, Magnetoelectric phase diagrams of orthorhombic $RMnO_3$ (R=Gd, Tb, and Dy), Phys. Rev. B 71 (2005), 224425, https://doi.org/10.1103/PhysRevB.71.224425.
[4] I.A. Sergienko, C. Sen, E. Dagotto, Ferroelectricity in the magnetic E-phase of orthorhombic perovskites, Phys. Rev. Lett. 97 (2006), 227204, https://doi.org/10.1103/PhysRevLett.97.227204.
[5] S. Picozzi, K. Yamauchi, B. Sanyal, I.A. Sergienko, E. Dagotto, Dual nature of improper ferroelectricity in a magnetoelectric multiferroic, Phys. Rev. Lett. 99 (2007), 227201, https://doi.org/10.1103/PhysRevLett.99.227201.
[6] S. Ishiwata, Y. Kaneko, Y. Tokunaga, Y. Taguchi, T.H. Arima, Y. Tokura, Perovskite manganites hosting versatile multiferroic phases with symmetric and antisymmetric exchange strictions, Phys. Rev. B 81 (2010).
[7] M. Kenzelmann, A.B. Harris, S. Jonas, C. Broholm, J. Schefer, S.B. Kim, C.L. Zhang, S.-W. Cheong, O.P. Vajk, J.W. Lynn, Magnetic inversion symmetry breaking and ferroelectricity in $TbMnO_3$ 087206, Phys. Rev. Lett. 95 (2005), https://doi.org/10.1103/PhysRevLett.95.087206.
[8] H.W. Brinks, J. Rodriguez-Carvajal, H. Fjellvag, A. Kjekshus, B.C. Hauback, Crystal and magnetic structure of orthorhombic $HoMnO_3$, Phys. Rev. B 63 (2001), 094411, https://doi.org/10.1103/PhysRevB.63.094411.
[9] A. Munoz, J.A. Alonso, M.T. Casais, M.J. Martinez-Lope, J.L. Martinez, M. T. Fernandez-Diaz, The magnetic structure of $YMnO_3$ perovskite revisited, J. Phys. Condens. Matter 14 (2002) 3285, https://doi.org/10.1088/0953-8984/14/12/315.
[10] B. Lorenz, Y.-Q. Wang, C.-W. Chu, Ferroelectricity in perovskite $HoMnO_3$ and $YMnO_3$, Phys. Rev. B 76 (2007), 104405, https://doi.org/10.1103/PhysRevB.76.104405.
[11] A.N. Matveeva, I.A. Zobkalo, M. Meven, A.L. Freidman, S.V. Semenov, K. Yu K. Terentjev, N.S. Pavlovskiy, M.I. Kolkov, K.A. Shaykhutdinov, V. Hutanu, Complex interplay between 3d and 4f magnetic systems in multiferroic $DyMnO_3$, J. Magn. Magn Mater. 569 (2023), 170415, https://doi.org/10.1016/j.jmmm.2023.170415.
[12] A. Munoz, M.T. Casais, J.A. Alonso, M.J. Martinez-Lope, J.L. Martinez, M. T. Fernandez-Diaz, Complex magnetism and magnetic structures of the metastable $HoMnO_3$ perovskite, Inorg. Chem. 40 (2001) 1020.
[13] H. Katsura, N. Nagaosa, A.V. Balatsky, Spin current and magnetoelectric effect in noncollinear magnets, Phys. Rev. Lett. 95 (2005), 057205, https://doi.org/10.1103/PhysRevLett.95.057205.
[14] I.A. Sergienko, E. Dagotto, Role of the Dzyaloshinskii-Moriya interaction in multiferroic perovskites, Phys. Rev. B 73 (2006), 094434, https://doi.org/10.1103/PhysRevB.73.094434.

[15] O. Prokhnenko, R. Feyerherm, E. Dudzik, S. Landsgesell, N. Aliouane, L.C. Chapon, D.N. Argyriou, Enhanced ferroelectric polarization by induced Dy spin order in multiferroic $DyMnO_3$, Phys. Rev. Lett. 98 (2007), 057206, https://doi.org/10.1103/PhysRevLett.98.057206.
[16] R. Feyerherm, E. Dudzik, O. Prokhnenko, D.N. Argyriou, Rare earth magnetism and ferroelectricity in $RMnO_3$ Journal of Physics: Conference Series 200 (2010), 012032, https://doi.org/10.1088/1742-6596/200/1/012032.
[17] H.W. Wang, C.L. Li, S.L. Yuan, J.F. Wang, C.L. Lu, J.-M. Liu, The crucial role of Mn spiral spin order in stabilizing the Dy–Mn exchange striction in multiferroic $DyMnO_3$, Phys. Chem. Chem. Phys. 19 (2017) 3706.
[18] C. Lu, J.-M. Liu, J. DyMnO, A model system of type-II multiferroics, Materiomics 2 (2016) 213, https://doi.org/10.1016/j.jmat.2016.04.004.
[19] I.A. Zobkalo, A.N. Matveeva, A. Sazonov, S.N. Barilo, S.V. Shiryaev, B. Pedersen, V. Hutanu, Direct control of magnetic chirality in $NdMn_2O_5$ by external electric field, Phys. Rev. B 101 (2020), 064425, https://doi.org/10.1103/PhysRevB.101.064425.
[20] M. Mochizuki, N. Furukawa, N. Nagaosa, Spin model of magnetostrictions in multiferroic Mn perovskites, Phys. Rev. Lett. 105 (2010), 037205, https://doi.org/10.1103/PhysRevLett.105.037205.
[21] N. Zhang, S. Dong, Z. Fu, Z. Yan, F. Chang, J. Liu, Multiferroic phase diagram of Y partially substituted Appl, Phys. Lett. 98 (2011), 012510, https://doi.org/10.1063/1.3536506.
[22] N. Zhang, Y.Y. Guo, L. Lin, S. Dong, Z.B. Yan, X.G. Li, J.-M. Liu, Ho substitution suppresses collinear Dy spin order and enhances polarization in $DyMnO_3$ Appl, Phys. Lett. 99 (2011), 102509, https://doi.org/10.1063/1.3636399.
[23] N. Zhang, S. Dong, J.-M. Liu, Ferroelectricity generated by spin-orbit and spin-lattice couplings in multiferroic $DyMnO_3$, Front. Physiol. 7 (2012) 408, https://doi.org/10.1007/s11467-011-0225-9.
[24] N. Lee, Y.J. Choi, M. Ramazanoglu, W. Ratcliff, V. Kiryukhin, S.-W. Cheong, Mechanism of exchange striction of ferroelectricity in multiferroic orthorhombic $HoMnO_3$ single crystals, Phys. Rev. B 84 (2011), https://doi.org/10.1103/PhysRevB.84.020101.
[25] S.V. Semenov, M.I. Kolkov, K.Y. Terent'ev, N.S. Pavlovskiy, M.S. Pavlovskiy, A. D. Vasiliev, A.V. Shabanov, K.A. Shaykhutdinov, D.A. Balaev, J. Supercond, Synthesis of the orthorhombic $Dy_{1-x}Ho_xMnO_3$ single crystals and study of their magnetic properties, nov, Magnesium 32 (2019) 3315, https://doi.org/10.1007/s10948-019-5090-8.
[26] V. Hutanu, Journal of large-scale research facilities, POLI: Polarised hot neutron diffractometer 1 (2015) A16, https://doi.org/10.17815/jlsrf-1-22.
[27] P.J. Brown, T. Chatterji, Neutron Scattering from Magnetic Materials, Elsevier Science, Amsterdam, 2006, pp. 215–244, https://doi.org/10.1016/B978-044451050-1/50006-9. CHAPTER 5 - Spherical Neutron Polarimetry.
[28] V. Hutanu, W. Luberstetter, E. Bourgeat-Lami, M. Meven, A. Sazonov, A. Steffen, G. Heger, G. Roth, E. Lelièvre-Berna, Implementation of a new Cryopad on the diffractometer POLI at MLZ, Rev. Sci. Instrum. 87 (2016), 105108, https://doi.org/10.1063/1.4963697.
[29] V. Hutanu, M. Meven, S. Masalovich, G. Heger, G. Roth, ^{3}He spin filters for spherical neutron polarimetry at the hot neutrons single crystal diffractometer POLI-HEiDi, J. Phys.: Conf. Series 294 (2011), 012012, https://doi.org/10.1088/1742-6596/294/1/012012.
[30] N. Aliouane, K. Schmalzl, D. Senff, A. Maljuk, K. Prokeš, M. Braden, and D. N. Argyriou. Flop of Electric Polarization Driven by the Flop of the Mn Spin Cycloid in Multiferroic TbMnO3 Phys. Rev. Let. 102, 207205, DOI:https://doi.org/10.1103/PhysRevLett.102.207205.
[31] A.L. Freidman, S.V. Semenov, M.I. Kolkov, K.Y. Terent'ev, N.S. Pavlovskiy, D. M. Gokhfeld, K.A. Shaykhutdinov, D.A. Balaev, Inverse and direct magnetoelectric effects in orthorhombic $DyMnO_3$ manganite single crystals, J. Appl. Phys. 128 (2020), 094102, https://doi.org/10.1063/5.0006595.
[32] J. Stein, M. Baum, S. Holbein, T. Cronert, V. Hutanu, A.C. Komarek, M. Braden, Control of multiferroic domains by external electric fields in $TbMnO_3$, J. Phys. Condens. Matter 27 (2015), 446001, https://doi.org/10.1088/0953-8984/27/44/446001.
[33] M. Matsubara, S. Manz, M. Mochizuki, T. Kubacka, A. Iyama, N. Aliouane, T. Kimura, S.L. Johnson, D. Meier, M. Fiebig, Magnetoelectric domain control in multiferroic $TbMnO_3$, Science (2015), https://doi.org/10.1126/science.1260561, 6239 1112.
[34] E. Bertaut, G. Rado, H. Suhl Magnetism, Academic Press vol. 3, 1963, p. 146.
[35] R. Feyerherm, E. Dudzik, A.U.B. Wolter, S. Valencia, O. Prokhnenko, A. Maljuk, S. Landsgesell, N. Aliouane, L. Bouchenoire, S. Brown, D.N. Argyriou, Magnetic-field induced effects on the electric polarization in $RMnO_3$(R=Dy,Gd), Phys. Rev. B 79 (2009), 134426, https://doi.org/10.1103/PhysRevB.79.134426.
[36] J. Rodriguez-Carvajal, Recent advances in magnetic structure determination by neutron powder diffraction, Physica B 192 (1993) 55, https://doi.org/10.1016/0921-4526(93)90108-I.
[37] Y. Yamasaki, H. Sagayama, T. Goto, M. Matsuura, K. Hirota, T. Arima, Y. Tokura, Electric control of spin helicity in a magnetic ferroelectric, Phys. Rev. Lett. 98 (2007), 147204, https://doi.org/10.1103/PhysRevLett.98.147204.
[38] M.M. Baum, PhD Thesis, University of Cologne, Germany, 2013.
[39] E.V. Milov, A.M. Kadomtseva, G.P. Vorob'ev, Yu F. Popov, V. Yu Ivanov, A. A. Mukhin, A.M. Balbashov, Switching of spontaneous electric polarization in the, $DyMnO_3$ multiferroic JETP Letters 85 (2007) 503, https://doi.org/10.1134/S0021364007100074.
[40] I.A. Zobkalo, S.V. Gavrilov, A. Sazonov, V. Hutanu, Investigation of $TbMn_2O_5$ by polarized neutron diffraction, J. Phys. Condens. Matter 30 (2018), 205804, https://doi.org/10.1088/1361-648X/aabdf6.
[41] N. Zhang, S. Dong, Z. Fu, Z. Yan, F. Chang, J. Liu, Phase transition and phase separation in multiferroic orthorhombic $Dy_{1-x}Ho_xMnO_3$ ($0 \leq x \leq 1$), Sci. Rep. 4 (2014) 6506, https://doi.org/10.1038/srep06506.